

Full paper

Highly efficient and stable inverted planar solar cells from (FAI)_x(MABr)_{1-x}PbI₂ perovskites

Weibo Yan^a, Haixia Rao^b, Chen Wei^b, Zhiwei Liu^b, Zuqiang Bian^{b,*}, Hao Xin^{a,*}, Wei Huang^{a,c,*}

^a Key Laboratory for Organic Electronics and Information Displays & Institute of Advanced Materials (IAM), Jiangsu National Synergetic Innovation Center for Advanced Materials (SICAM), Nanjing University of Posts & Telecommunications, 9 Wenyuan Road, Nanjing 210023, China

^b State Key Laboratory of Rare Earth Materials Chemistry and Applications, College of Chemistry and Molecular Engineering, Peking University, Beijing 100871, China

^c Key Laboratory of Flexible Electronics (KLOFE) & Institute of Advanced Materials (IAM), Jiangsu National Synergetic Innovation Center for Advanced Materials (SICAM), Nanjing Tech University (NanjingTech), 30 South Puzhu Road, Nanjing 211816, China

ARTICLE INFO

Keywords:

Inverted perovskite solar cells
Bromine-doped perovskites
(FA)_y(MA)_{1-y}PbBr_xI_{3-x}
Enlarged bandgaps
Enhanced open-circuit voltages
Broadened absorption spectra

ABSTRACT

We report highly efficient and stable inverted planar lead mixed-halide (Br, I) perovskite solar cells with a configuration of ITO/poly(3-bromothiophene)/(FA)_y(MA)_{1-y}PbBr_xI_{3-x}/C₆₀/BCP/Ag (FA: HC(NH₂)₂⁺; MA: CH₃NH₃⁺). We found that small changes in the composition of (FA)_y(MA)_{1-y}PbBr_xI_{3-x} have big impact on the material properties and device performance. Appropriate Br-doping enlarges MAPbBr_xI_{3-x}'s bandgaps and prolongs the life of the excited charge carrier, which leads to higher device open-circuit voltage (V_{OC}). Replacing "MA" with "FA" extends the absorption of (FA)_y(MA)_{1-y}PbBr_xI_{3-x} which compensates the J_{SC} loss in MAPbBr_xI_{3-x} from Br-doping. The optimized perovskite film with a composite of FA_{0.8}MA_{0.2}PbBr_{0.2}I_{2.8} shows a lifetime of 670 ns and a photoelectric response to 830 nm, resulting in an enhanced J_{SC} of 22.2 mA cm⁻², a high FF of 0.80, and an efficiency of 18.1%. In addition, the inverted device based on FA_{0.8}MA_{0.2}PbBr_{0.2}I_{2.8} showed long-term stability with 80% efficiency remained after 4 months in a glovebox without encapsulation. Our results demonstrate highly efficient and stable inverted planar perovskite solar cells can be achieved by optimizing absorber material composition, which offer a reference for their applications in flexible or tandem solar cells.

1. Introduction

The performance of perovskite solar cells (PSCs) still has large room for further improvement considering its theoretical efficiency [1]. The optimization of perovskite film quality [2–7] and the use of interfacial materials to enhance charge collection [8–12] have achieved desirable effect on device efficiency [2,3,5]. Another important strategy to improve performance is the optimization of perovskite absorber material composition, which can be divided into two aspects, 1) Cl [12,13] or Br [14,15] doping. As early as 2013, Sang Il Seok et al. had demonstrated that the band-gap of MAPbX₃ can be tuned via replacing I with Br ions, which covered almost the entire visible spectrum [16]. MAPbX_bI_{3-b} (X=Cl, Br) have many advantages compared to MAPbI₃. First, they show longer charge carrier diffusion length [17,18], which can reduce charge recombination rate and enable the use of thicker layer to absorb more light; Second, they have wider bandgaps which increase device open-circuit voltage (V_{OC}) [8,13,15]; third, they are theoretically more stable than MAPbI₃ because of increased motivating

factors [19]. Recent results reveal that Br-doping has greater potential than Cl-doping because Br-doping can adjust perovskite composition in a wider range [15], thus can tune device parameters including V_{OC} and J_{SC} in a broader extent. 2) Partially substitution of methyl ammonium (MA: CH₃NH₃⁺) by formamidinium (FA: HC(NH₂)₂⁺) [20], which extends the absorption edge to longer wavelength and thus improves J_{SC} [20]. The combination of these two substitutions can balance the V_{OC} and J_{SC} of the device and has shown huge potential in regular mesoporous PSCs [15]. An efficiency of 18.4% with a V_{OC} of 1.11 V was achieved in perovskite (FAPbI₃)_{0.85}(MAPbBr₃)_{0.15} with a device architecture of FTO/blocking-TiO₂/mesoporous-TiO₂:perovskite-composite layer/perovskite upper layer/PTAA/Au [15]. Later, by fine composition tuning, an efficiency as high as 20.8% was obtained from (FA)_{4/6}(MA)_{2/6}PbBr_{0.5}I_{2.5} with a J_{SC} of 24.6 mA cm⁻², a V_{OC} of 1.16 V, and a FF of 0.73 [21,22].

However, the applications of MAPbX_bI_{3-b} or (FA)_y(MA)_{1-y}PbBr_xI_{3-x} in inverted planar devices are rare, mainly due to unfeasible formation of high quality crystalline films via solution

* Corresponding authors.

E-mail addresses: iamhxin@njupt.edu.cn (H. Xin), iamwhuang@njtech.edu.cn (W. Huang).

process in the absence of mesoporous-TiO₂ scaffold [23]. Inverted planar PSCs have many advantages compared to regular structured ones, such as suitable for fabricating low-temperature solution-processable devices, compatible with flexible substrates and solution processed interfacial materials [12]. Thus, it is important to develop inverted planar PSCs using the lead mixed-bromine perovskites as the absorber layer. In the previous work [24], some of the authors have successfully fabricated poly(3-bromothiophene) (PBT) film as a hole-selective layer for inverted planar PSCs. The results showed that PBT is very compatible with perovskite precursor solution and feasible for crystalline film formation atop it. In this work, by using PBT as the interfacial layer, high quality Br-doped perovskite films were achieved and inverted planar PSCs were fabricated. The effect of the composition of FA_xMA_{1-y}PbBr_xI_{3-x} on inverted device performance was systematically studied and a power conversion efficiency as high as 18.1% was achieved from perovskite with a composition of FA_{0.8}MA_{0.2}PbBr_{0.2}I_{2.8}.

2. Materials and methods

2.1. Materials

3-bromothiophene and BF₃.Et₂O were purchased from Zhongshenghuateng Company. BF₃.Et₂O was purified by distillation prior to use. PbI₂, C₆₀, and BCP were purchased from Alfa Aesar and Ag was purchased from Sigma-Aldrich. PdI₂, C₆₀ and BCP were purified by vacuum sublimation. CH₃NH₃I was synthesized according to the literature [10] and recrystallized prior to use. Indium tin oxide (ITO) coated glass substrates with a sheet resistance of 24 Ω/sq were purchased from CSG Holding Co., Ltd.

2.2. Instrumentations

UV-vis spectra were obtained with a Lambda 35 spectrophotometer. The bandgaps of hole-transporting material (HTM) and perovskite samples were determined by the absorption edge ($E_g=1240/\lambda_{eg}$). The work functions [the highest occupied molecular orbital (HOMO) energy levels] of HTM and perovskite samples were measured on an ultraviolet photoelectron spectroscopy (UPS) (Ac-2, Riken Keiki). The lowest unoccupied molecular orbital (LUMO) of HTM and perovskite samples were calculated from E_{HOMO} and E_g ($E_{LUMO}-E_{HOMO}=E_g$). XRD patterns were performed on a Rigaku D/max-2500 X-ray diffractometer with Cu-Kα radiation at a generator voltage of 40 kV and a current of 100 mA. Scanning electron microscope (SEM) images were measured on Hitachi S-4800 SEM microscope. Fluorescence spectra of the perovskite films were recorded with a Fluora Max-3P spectra photometer with an exciting wavelength of 466 nm. The time-resolved PL was recorded at the peak emission of around 750 nm by a lifetime and steady state spectrometer (FLS980, Edinburgh Instruments Ltd.) with a 470 nm laser.

2.3. Synthesis of poly(3-bromothiophene) (PBT)

PBT films were synthesized in a one-compartment cell under computer control in a three-electrode test system according to the reference [24,25]. ITO glass substrate (~0.38 cm×2.2 cm), platinum wire (which was placed 0.5 cm apart from ITO) and Ag/AgCl electrode were served as the working electrode, counter electrode, and reference electrode, respectively. The electrolyte solution was freshly distilled BF₃.Et₂O containing 30 mM biphenyl monomer. The solutions were degassed with a stream of dry argon before electrochemical reaction and a slight overpressure was maintained during each experiment. The PBT films were grown at +1.40 V and the polymerization current was 1.00×10⁻⁴ A and reaction time was 10 s. After polymerization, the films were thoroughly rinsed with diethyl ether and ethanol, and then dried under nitrogen flow.

2.4. Preparation of the lead mixed-halide precursor solutions

The precursor solutions of MAPbBr_xI_{3-x} (x=0.2 to 3.0) were prepared by dissolving MABr, MAI, and PbI₂ (or MABr, PbI₂ and PbBr₂) in N,N-dimethylformamide (DMF) with defined stoichiometry and concentration. The precursor solutions of (FAI)_x(MABr)_{1-x}PbI₂ (x=0.8, 0.6 and 0.4) were prepared by dissolving MABr, FAI, and PbI₂ in DMF with defined stoichiometry and concentration.

2.5. Device fabrication and photovoltaic characterization

Lead mixed-halide perovskite films were fabricated according to the one-step fast deposition-crystallization procedure [10]. Lead mixed-halide precursor solution was first spin-coated on top of PBT/ITO at 5000 rpm for 4–6 s, followed by immediate exposure to chlorobenzene to induce crystallization, and then spin at 5000 rpm for 60 s. The film was annealed at a set temperature for 10 min before it was loaded into a vacuum chamber for the thermal deposition of 40 nm C₆₀ and 10 nm BCP. Finally, Ag (100 nm) was thermally evaporated on top of the device to form the back contact. The current density-voltage (J-V) curves of photovoltaic devices were obtained by a Keithley 4200 source-measure unit with forward scanning direction from -0.2 to 1.3 V and reverse direction from 1.3 to -0.2V at different sweep rates. The photocurrent and device stability was measured under simulated 100 mW cm⁻² AM 1.5G irradiation using a xenon-lamp-based solar simulator [Oriol 300W solar simulator Thermo Oriol 91160-1000]. All the device fabrication and characterization were performed in nitrogen filled glove box with oxygen level at about 100 ppm and water content about 0.01 ppm.

3. Results and discussion

We first conducted a solely Br-doping of MAPbI₃ in order to enlarge perovskite's bandgap and increase device V_{OC} [26]. Fig. 1a shows the absorption and the tauc plots of MAPbBr_xI_{3-x} with x=0, 0.2, 0.4, and 0.6. The detailed absorption spectra of MAPbBr_xI_{3-x} films as well as their photos with x changing from 0.2 to 3.0 are given in Fig. S1 and S2. As expected, the absorption edge gradually blue shifted with the increase of Br content (x) and the bandgaps of MAPbBr_xI_{3-x} absorber materials extrapolated from the tauc plots are 1.60, 1.63, 1.67, 1.70 eV for x=0, 0.2, 0.4, 0.6, respectively. The band gap for MAPbBr₃ is 2.3 eV. The HOMO energy levels of MAPbBr_xI_{3-x} obtained from the ultraviolet photoelectron spectra (Fig. S3) varies between -5.4 eV and -5.7 eV (Table S1).

The crystalline structure of MAPbBr_xI_{3-x} perovskite film on the PBT/ITO/glass substrate was characterized by glancing angle X-ray diffraction (GAXRD) and the results are shown in Fig. 1b and S4. The main diffraction peaks of MAPbI₃ at 14.1°, 28.4°, 31.9° and 40.6°, being assigned to 110, 220, 310 and 330 diffractions, gradually shifted to higher angle (14.2°, 28.7°, 31.2° and 41.0°, respectively for MAPbBr_{0.6}I_{2.4}) with the increase of the Br doping concentration, which indicates the successful doping of Br into the lattice of MAPbI₃ and agrees well with the variation of the bandgaps [27].

The PL peaks of MAPbBr_xI_{3-x} perovskite exhibited intrinsic fluorescence emission at 760 (x=0.2), 751 (x=0.4) and 727 nm (x=0.6), which is blue-shifted with the increase of Br-doping extent (Fig. S5). Time resolved photoluminescence (TRPL) was characterized to probe the charge lifetime of the obtained MAPbBr_xI_{3-x} (x=0.2, 0.4, 0.6) perovskites. Fig. 1c shows the TRPL spectra recorded at their peak emission by 470 nm laser excitation from the pristine films deposited on nonconductive glass substrate. All the curves can be fitted with a single exponential decay function and the lifetimes are calculated to be 41.3, 141.9, and 56.9 ns for x=0.2, x=0.4, and x=0.6, respectively. The results demonstrate that longer charge carrier life can be achieved at certain Br-doping degree in MAPbI₃ perovskites, which resembles that of Cl-doping. The prolonged charge carrier lifetime also indicates that

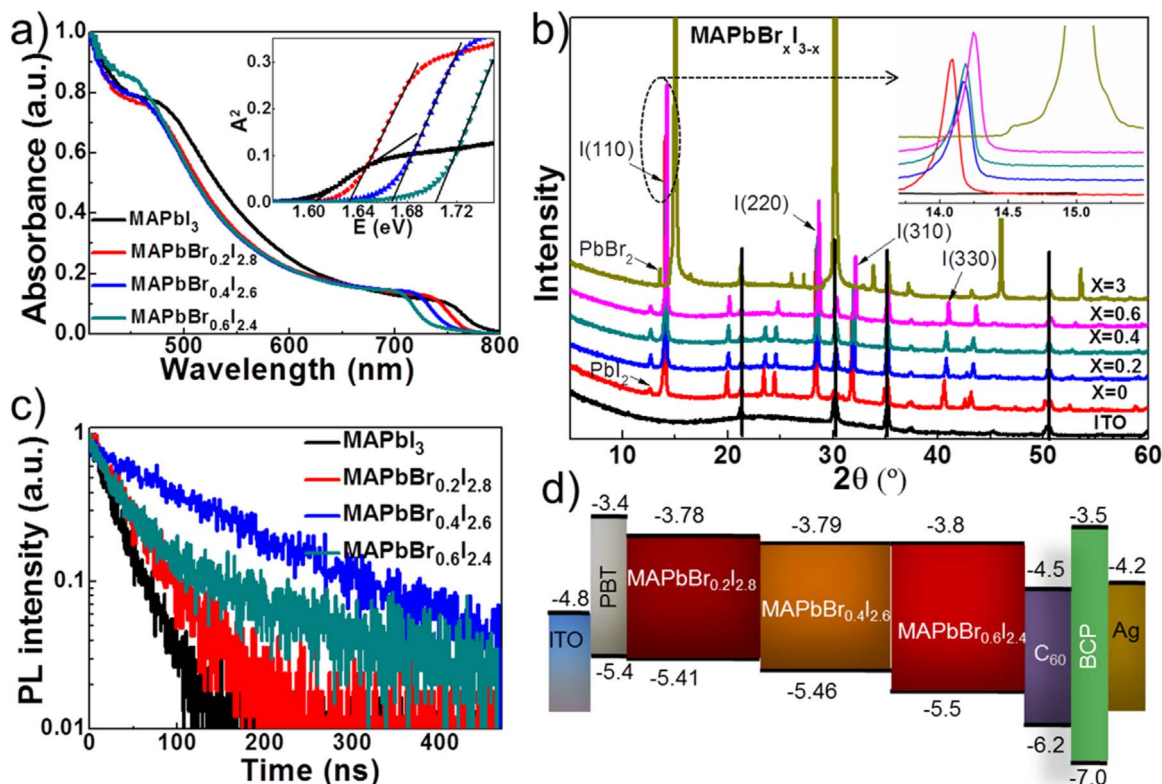


Fig. 1. a) UV-vis absorption of MAPbBr_xI_{3-x} perovskites films. Insert: Tauc plots and the linear extrapolation of the band gaps; b) XRD patterns of MAPbBr_xI_{3-x} films measured on PBT/ITO/glass. Insert shows zoomed in (110) peaks for better comparison. The pattern of PBT/ITO/glass is also shown for reference; c) TRPL of MAPbBr_xI_{3-x} (x = 0, 0.2, 0.4, 0.6). Samples were deposited on nonconductive glass substrates; d) Energy levels of MAPbBr_xI_{3-x} and other materials used in the inverted PSCs.

high crystalline MAPbBr_xI_{3-x} films were successfully fabricated [21]. Compared to pure MAPbBr_{0.4}I_{2.6} film, a clear PL quenching was observed in MAPbBr_{0.4}I_{2.6}/PBT film (Fig. S4) confirming efficient hole-transfer from MAPbBr_{0.4}I_{2.6} absorber layer to PBT interfacial layer [27]. PBT has a HOMO of -5.4 eV (Fig. 1d), matching well with that of the MAPbBr_xI_{3-x} perovskites [27]. Therefore, it can effectively extract hole from perovskite material and facilitates the hole-transfer to ITO anode.

Inverted planar perovskite solar cells with a structure of ITO/PBT/MAPbBr_xI_{3-x}/C₆₀/BCP/Ag were fabricated using previous reported process [24]. The current density-voltage (J-V) curves of the whole set of devices (x = 0–3.0) are given in Fig. S6. With the increase of Br-doping concentration (from x = 0.2 to x = 3.0), the V_{OC} of the devices first increases then decreases and reaches a maximum of 1.2 V for x = 2.2, whereas the J_{SC} continuously decreases due to the weakening of the light-absorption ability stemming from the narrowing of photo-absorption region (Fig. S2). The three highest efficiencies are achieved with x = 0.2, 0.4 and 0.6 and their J-V curves and external quantum efficiency (EQE) are shown in Fig. 2a and b, respectively. The V_{OC}, J_{SC}, FF, and PCE are 1.02, 1.05, and 1.09 V, 21.1, 20.7, and 19.5 mA cm⁻², 0.77, 0.73, and 0.65, 16.6%, 15.9%, and 13.8% for x = 0.2, 0.4, and 0.6, respectively. The J_{SC} measured from the J-V curves match well with that integrated from the EQE, which are 20.0, 19.4, and 18.8 mA cm⁻² for x = 0.2, 0.4, and 0.6, respectively. In consideration of the device performance and charge carrier lifetime (Fig. 1c), MAPbBr_{0.4}I_{2.6} was selected for further device optimization [15]. The J-V curves of MAPbBr_{0.4}I_{2.6} based solar cells with the films annealed at different temperature are shown in Fig. 2c and the device parameters are summarized in Table 1. It can be seen that with increase of the annealing temperature, device V_{OC}, J_{SC} and FF first increase and then decrease with the highest efficiency of 17.3% observed at an annealing temperature of 110 °C. Fig. 2d shows that its PCE values are in agreement with that obtained from the stabilized power output near

the maximum power point, reflecting the device performance in the working condition more closely.

To further understand the relationship between the device performance and film quality, SEM was conducted and the images are shown in Fig. 3. High-quality crystalline films of MAPbI₃ (Fig. 3a), MAPbBr_{0.2}I_{2.8} (Fig. 3b), MAPbBr_{0.4}I_{2.6} (Fig. 3c), and MAPbBr_{0.6}I_{2.4} (Fig. 3d) were observed at the annealing temperature of 100 °C, which ensures the rationality of device performance comparison based on these three perovskites. When the annealing temperature increased from 100 to 110 °C for MAPbBr_{0.4}I_{2.6}, large and well connected grains are observed without any pinholes (Fig. 3e), consistent with the device performance improvement (Fig. 2c). With the temperature further increased to 120 °C and 130 °C, pinholes and cracks appeared (Fig. 3f and g), which explain the decline of the device performance.

Considering the relatively low J_{SC} of the champion cell based on MAPbBr_xI_{3-x}, “FA” was induced to partially replace “MA” in order to broaden the absorption spectrum into infrared region. The UV-vis spectra of (FAI)_x(MABr)_{1-x}PbI₂ (x = 0.4, 0.6, 0.8, 1.0) are shown in Fig. 4a. As expected, the absorption of (FAI)_x(MABr)_{1-x}PbI₂ is broadened with the increase of “FA” content and the onset of the absorption for x = 0.4, 0.6, 0.8, and 1.0 are 747, 788, 811 and 832 nm, respectively.

The crystalline structure of (FAI)_x(MABr)_{1-x}PbI₂ perovskite film on the PBT/ITO/glass substrate was further analyzed by GAXRD and the results are shown in Fig. 4b. The main diffraction peaks of MAPbBrI₂ [(FAI)_x(MABr)_{1-x}PbI₂, x = 0] at 14.5°, 20.3°, 24.9°, 29.0°, 32.4°, 41.3° and 44.0°, being assigned to the 110, 112, 211, 220, 310, 330 and 224 diffractions, gradually shifted to lower angles with increase of “FA” content and they are 13.8°, 19.7°, 24.3°, 28.1°, 31.6°, 40.2° and 42.6° for FAPbI₃ [(FAI)_x(MABr)_{1-x}PbI₂, x = 1].

The gradual shift in the diffraction angle is a strong indication that a mixed phase of (FAI)_x(MABr)_{1-x}PbI₂ is formed in which “FA” and “MA” cations are both inserted in the same lattice frame [15]. The PL

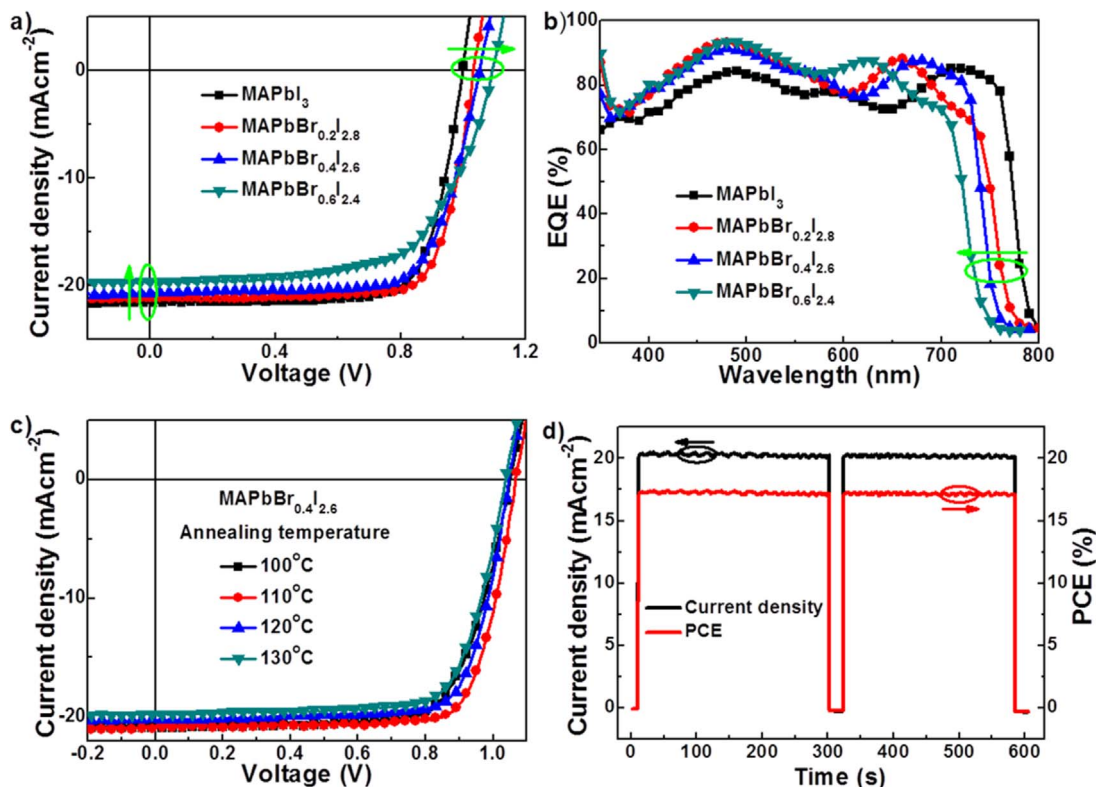


Fig. 2. a) J–V curves of the best performing MAPbBr_xI_{3–x} solar cells with different Br substitution. All the films were annealed at 100 °C; b) EQE spectrum of the devices in (a); c) J–V curves of MAPbBr_{0.4}I_{2.6} solar cells with the absorber film annealed at different temperature; d) photocurrent density and PCE of the champion MAPbBr_{0.4}I_{2.6} solar cell as a function of time measured at a forward bias of 0.85 V. The cell was placed in the darkness prior to the measurement and the light was turned off for 20 s after working for 300 s. All the devices had a configuration of ITO/PBT/MAPbBr_xI_{3–x}/C₆₀/Ag and were measured under simulated 100 mW cm^{–2} AM1.5 sun light.

peaks of (FAI)_x(MABr)_{1–x}PbI₂ perovskite exhibit intrinsic fluorescence emission at 748 (x=0.4), 773 (x=0.6), and 796 (x=0.8) nm, which is red-shifted with the increase of “FAI” extent and decrease of “MABr” (Fig. S7). TRPL spectra (Fig. 4c) for these three materials were recorded at their maximum emission and PL lifetimes for (FAI)_x(MABr)_{1–x}PbI₂ being fitted with a single exponential decay function are 331.6 (x=0.4), 182.2 (x=0.6), 670.0 (x=0.8), and 179.6 (x=1.0), respectively. Compared with the lifetimes of MAPbBr_xI_{3–x}, 41.3 ns for x=0.2, 141.9 ns for x=0.4, and 56.9 ns for x=0.6, the lifetimes of (FAI)_x(MABr)_{1–x}PbI₂ are greatly improved after “FA” substitution in Br-doped perovskites. This means excitons in the (FAI)_x(MABr)_{1–x}PbI₂ films can travel longer distance and more excitons can reach the interfaces of perovskite/HTM and perovskite/ETM. The long lifetime also indicates high-quality (FAI)_x(MABr)_{1–x}PbI₂ crystalline films were formed, which can reduce exciton recombination and enhance charge collection. In addition, a clear PL quenching was observed in (FAI)_{0.8}(MABr)_{0.2}PbI₂/PBT film compared to that without PBT (Fig. S7), confirming efficient hole-transfer from (FAI)_{0.8}(MABr)_{0.2}PbI₂ to PBT.

Fig. 4d shows the HOMO and LUMO energy levels of (FAI)_x(MABr)_{1–x}PbI₂ (x=0.4, 0.6, 0.8). Compared to MAPbBr_xI_{3–x} (Fig. 1d), “FA” substitution slightly lowers the HOMOs and LUMOs

of the perovskites. With the increase of “FA” content, the bandgaps of (FAI)_x(MABr)_{1–x}PbI₂ become narrower with the LUMO remains nearly unchanged and the HOMOs goes up slightly. The lower LUMO increases the gap of LUMOs between perovskite and HTM (PBT) and could enhance the electron-blocking ability of PBT. The approaching of the HOMO of (FAI)_x(MABr)_{1–x}PbI₂ to that of PBT is beneficial for hole-transfer from (FAI)_x(MABr)_{1–x}PbI₂ to PBT.

Based on the correlation between the device performance and the stoichiometry of MAPbBr_xI_{3–x} (MAPbBr_xI_{3–x}; x=0.2, 0.4, 0.6) perovskites (Fig. S6, Table S2), the device optimization of (FAI)_x(MABr)_{1–x}PbI₂ are focused on that with x=0.4, 0.6 and 0.8. The results are shown in Fig. 5 and the device parameters are summarized in Table 2. The initially annealing temperature of these perovskite films were set at 130 °C according to the literature [15].

From Table 2, it is obvious that under the same annealing condition, with the increase of “FAI”, the average J_{SC} increases from 17.4 to 20.9 mA cm^{–2} and to 21.8 mA cm^{–2} and the V_{OC} decreases from 1.07 to 1.04 and to 1.01 V for x=0.4, 0.6, and 0.8, respectively. The V_{OC} , J_{SC} , FF, and PCE from their corresponding champion devices are 1.06, 1.04, and 1.02 V, 17.8, 20.9, and 22.2 mA cm^{–2}, 0.72, 0.77, and 0.80, 13.6%, 16.7%, and 18.1% for x=0.4, 0.6, and 0.8, respectively (Fig. 5a). This variation agrees well with the calculated J_{SC} from the

Table 1.

The annealing temperature effect on device performance of MAPbBr_{0.4}I_{2.6} perovskite.

Perovskites ^a	Annealing temperature (°C)	V_{OC} (V)	J_{SC} (mA cm ^{–2})	FF	PCE (%)
MAPbBr _{0.4} I _{2.6}	100	1.05 (± 0.02)	20.5 (± 0.6)	0.74 (± 0.04)	16.0 (± 0.7)
	110	1.06 (± 0.02)	20.7 (± 1.0)	0.76 (± 0.03)	16.5 (± 0.8)
	Champion	1.07	20.6	0.784	17.3
	120	1.05 (± 0.01)	19.9 (± 1.2)	0.75 (± 0.02)	15.6 (± 1.0)
	130	1.03 (± 0.01)	19.3 (± 1.0)	0.72 (± 0.03)	14.5 (± 1.1)

^a The thickness of the perovskite active layer is 260 ± 25 nm for all devices. The average value was calculated from ~50 devices.

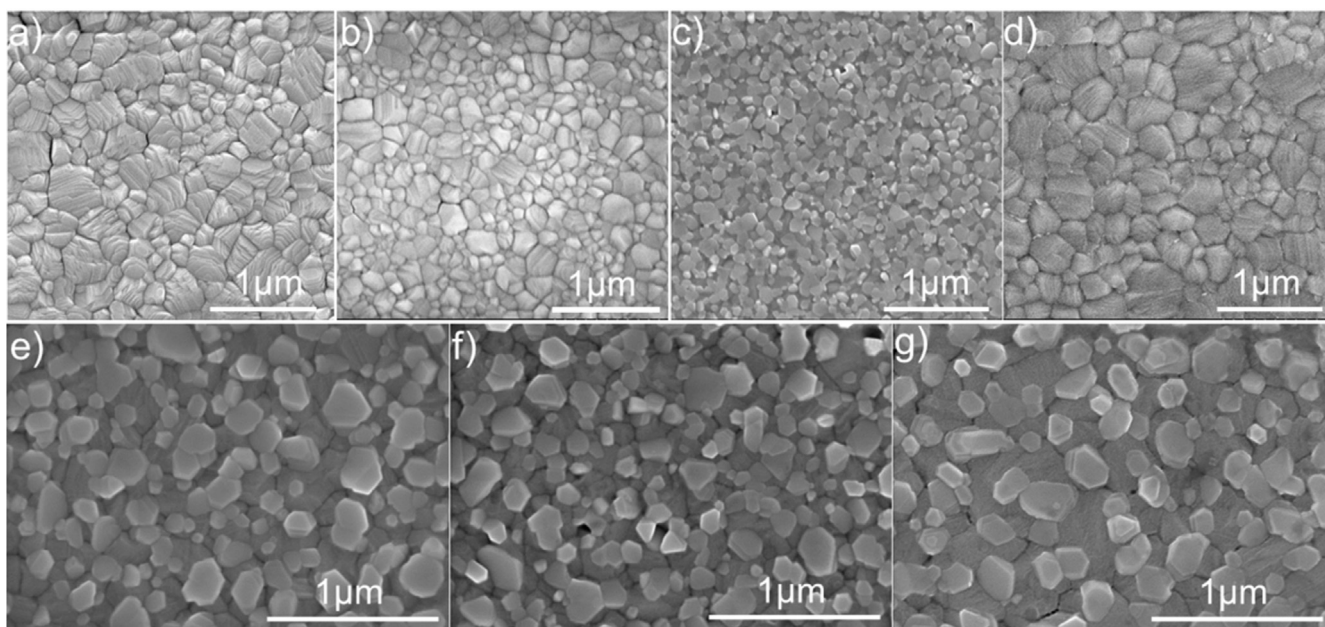


Fig. 3. SEM images of MAPbBr_xI_{1-x} ($x=0, 0.2, 0.4, 0.6$) films annealed at different temperature. All films were deposited on PBT/ITO glass substrates. a) $x=0, 100\text{ }^{\circ}\text{C}$; b) $x=0.2, 100\text{ }^{\circ}\text{C}$; c) $x=0.4, 100\text{ }^{\circ}\text{C}$; d) $x=0.6, 100\text{ }^{\circ}\text{C}$; e) $x=0.4, 110\text{ }^{\circ}\text{C}$; f) $x=0.4, 120\text{ }^{\circ}\text{C}$; g) $x=0.4, 130\text{ }^{\circ}\text{C}$.

EQE, 16.6, 19.3 and 20.2 mA cm^{-2} for the devices based on $x=0.4$, $x=0.6$ and $x=0.8$, respectively, as shown in Fig. 5b. With the increase of “FAI”, the edges of EQE curves are red-shifted from 754 ($x=0.4$) to 793 ($x=0.6$) and to 818 ($x=0.8$) nm, which is consistent with absorption variation (Fig. 4a). We further changed the annealing temperature of the best performing (FAI)_{0.8}(MABr)_{0.2}PbI₂ films to 120 and 140 °C and no device further improvement was obtained (Fig. 5c and Table 2).

Thus, the champion PCE of 18.1% is achieved from (FAI)_{0.8}(MABr)_{0.2}PbI₂ with a V_{OC} of 1.02 V, a J_{SC} of 22.2 mA cm^{-2} and a FF of 0.80. The PCE values are in agreement with that obtained from the stabilized power output near the maximum power point, indicating future available practical application with high performance in the working condition, as displayed in Fig. 5d.

The hysteresis character of the champion inverted planar solar cells

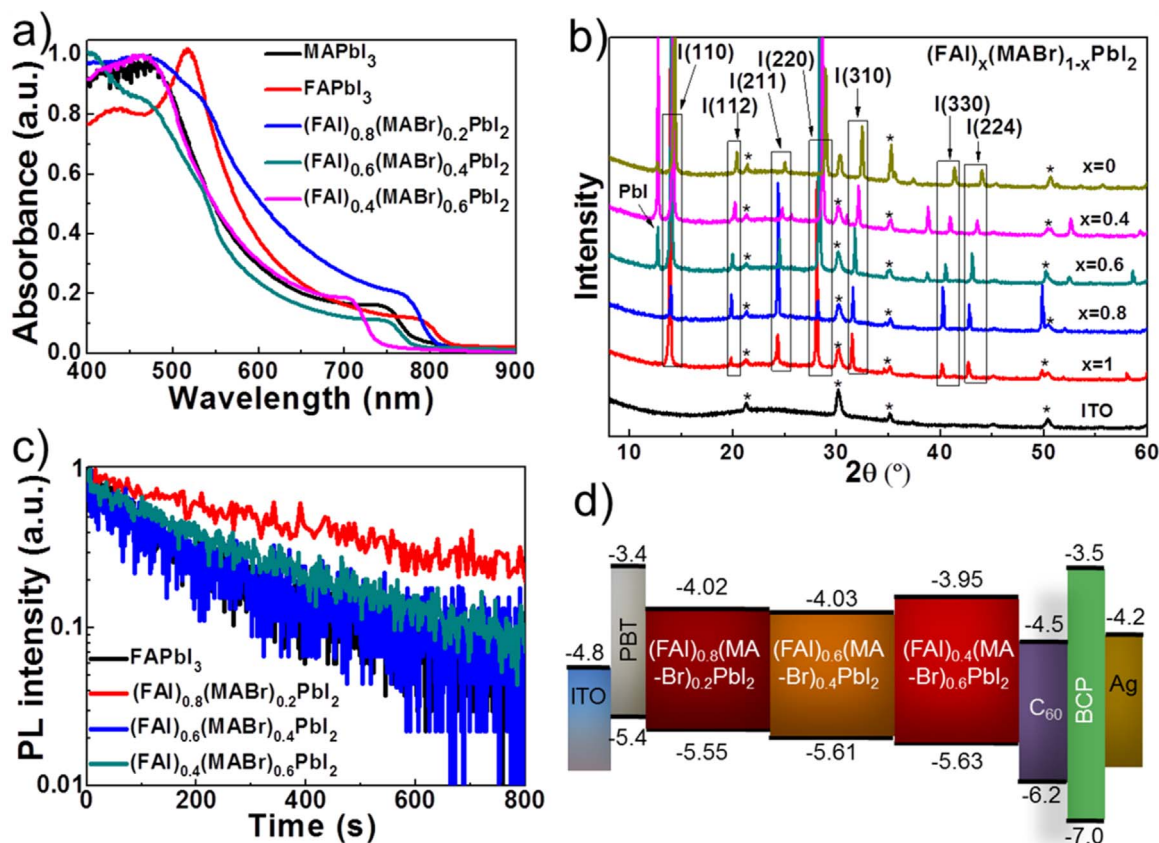


Fig. 4. a) Absorption spectra of (FAI)_x(MABr)_{1-x}PbI₂ perovskite films; b) XRD patterns of (FAI)_x(MABr)_{1-x}PbI₂ measured on PBT/ITO/glass; c) TRPL of (FAI)_x(MABr)_{1-x}PbI₂ ($x=0.8, 0.6, 0.4$). Samples were deposited on nonconductive glass; d) energy levels of (FAI)_x(MABr)_{1-x}PbI₂ and other materials used in the inverted PSCs.

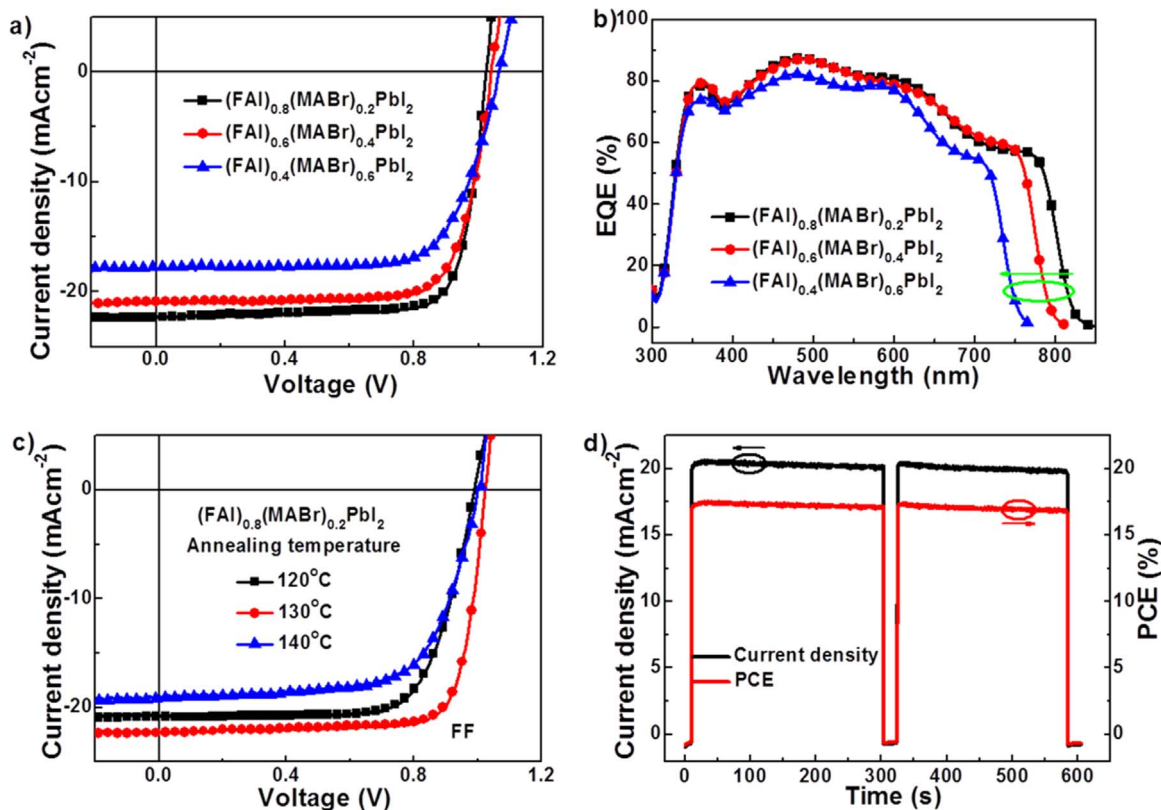


Fig. 5. a) J–V curves of the best performing $(\text{FAI})_x(\text{MABr})_{1-x}\text{PbI}_2$ solar cells with different FAI and MABr constitute. All the films were annealed at 130 °C. b) EQE spectrum of the devices in (a); c) J–V curves of $(\text{FAI})_{0.8}(\text{MABr})_{0.2}\text{PbI}_2$ solar cells at different annealing temperature; d) photocurrent density and PCE of the champion $(\text{FAI})_{0.8}(\text{MABr})_{0.2}\text{PbI}_2$ solar cell as a function of time measured at a forward bias of 0.85 V. The cell was placed in the darkness prior to the measurement and the light was turned off for 20 s after working for 300 s. All the devices had a configuration of ITO/PBT/FAI_x(MABr)_{1-x}PbI₂/C₆₀/Ag and were measured under simulated 100 mW cm⁻² AM1.5 sun light.

of $(\text{FAI})_{0.8}(\text{MABr})_{0.2}\text{PbI}_2$ was tested and the J–V curves measured at scanning rates from 100 to 500 mV/s with different scanning direction are given in Fig. S9. No large variation of efficiency is observed at different scanning rates (Fig. S9a) or directions (Fig. S9b), demonstrating very weak hysteresis in this device. This is believed due to balanced electron flux (J_e) and hole flux (J_h) to anode and cathode [28] and is beneficial for charge collection.

To further understand the relationship between the device performance and film quality, SEM was conducted and the images are given in Fig. 6. Large condensed crystalline grains with micro sizes were observed in all films at the annealing temperature of 130 °C (Fig. 6a–c), which ensures the rationality of performance comparison based on these three perovskite materials. When the annealing temperature decreased from 130 to 120 °C for $(\text{FAI})_{0.8}(\text{MABr})_{0.2}\text{PbI}_2$, smaller grains are observed (Fig. 6d), and more boundaries formed, which increase exciton recombination rate, leading to the device performance decline (Fig. 5c). With the temperature increased to 140 °C, obvious cracks appeared (Fig. 6f), which explains the dramatically decline of the device performance.

To explore the stability of the inverted planar solar cell based on

$(\text{FAI})_x(\text{MABr})_{1-x}\text{PbI}_2$ perovskites, the champion device without any encapsulation was tested in a N₂-glovebox with the oxygen about 100 ppm, water about 0.01 ppm and a temperature about 30 °C. As shown in Fig. 7, no obvious change of the four key photovoltaic parameters, V_{OC} , J_{SC} , FF, and PCE were observed within two weeks. We believe “FA” and “Br” doping improves the stability of the perovskite. Partially substitution of “MA” by slightly larger “FA” gives rise of Goldschmidt tolerance factor (t_f) closer to unity and the substitution of “I” atoms with smaller “Br” atoms leads to a reduction of the lattice constant, which results in a transition of the perovskite structure to a stable, compact cubic phase and improve its stability to moisture and temperature [29].

After four months, the PCE of the device showed a 20% drop from 18.1% to 14.5% (Fig. 7d), mainly due to the decrease of FF from 0.80 to 0.70 and J_{SC} from 22.2 mA cm⁻² to 19.8 mA cm⁻². This is probably due to gradual corrosion of the perovskite absorber materials and the electrodes due to long time exposure to trace O₂ and moisture in the glovebox. We expect less efficiency drop with encapsulation.

Table 2.

The constitute effect on photovoltaic performance of $(\text{FAI})_x(\text{MABr})_{1-x}\text{PbI}_2$ based devices and the annealing temperature effect on $(\text{FAI})_{0.8}(\text{MABr})_{0.2}\text{PbI}_2$ based devices.

Perovskites ^a	Annealing temperature (°C)	V_{OC} (V)	J_{SC} (mA cm ⁻²)	FF	PCE (%)
$(\text{FAI})_{0.4}(\text{MABr})_{0.6}\text{PbI}_2$	130	1.07(±0.02)	17.4(±0.8)	0.70(±0.08)	13.1(±1.0)
$(\text{FAI})_{0.6}(\text{MABr})_{0.4}\text{PbI}_2$	130	1.04(±0.02)	20.9(±0.9)	0.73(±0.05)	16.0(±1.2)
$(\text{FAI})_{0.8}(\text{MABr})_{0.2}\text{PbI}_2$	120	0.94(±0.05)	19.9(±1.0)	0.67(±0.06)	13.5(±1.4)
	130	1.01(±0.03)	21.8(±1.0)	0.76(±0.05)	16.9(±1.2)
	Champion	1.02	22.2	0.798	18.1
	140	0.97(±0.03)	18.2(±2.0)	0.66(±0.08)	12.0(±1.1)

^a Film thicknesses for x=0.4, 0.6, 0.8 are 250 ± 30 nm, 260 ± 30 nm and 260 ± 35 nm, respectively. The average value was calculated from ~50 devices.

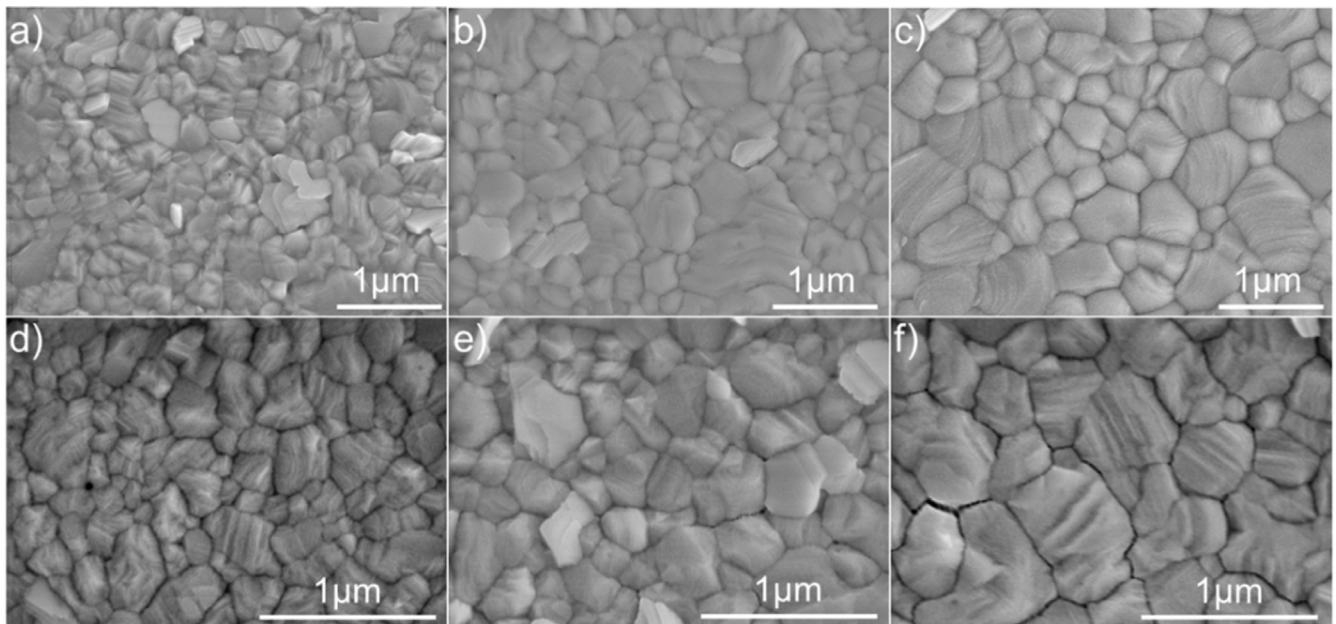


Fig. 6. SEM micrographs of $(\text{FAI})_x(\text{MABr})_{1-x}\text{PbI}_2$ films measured on PBT/ITO glass substrates with different annealing temperature. a) $x=0.8$, 130 °C; b) $x=0.6$, 130 °C; c) $x=0.4$, 130 °C; d) $x=0.8$, 120 °C; e) $x=0.8$, 130 °C; f) $x=0.8$, 140 °C.

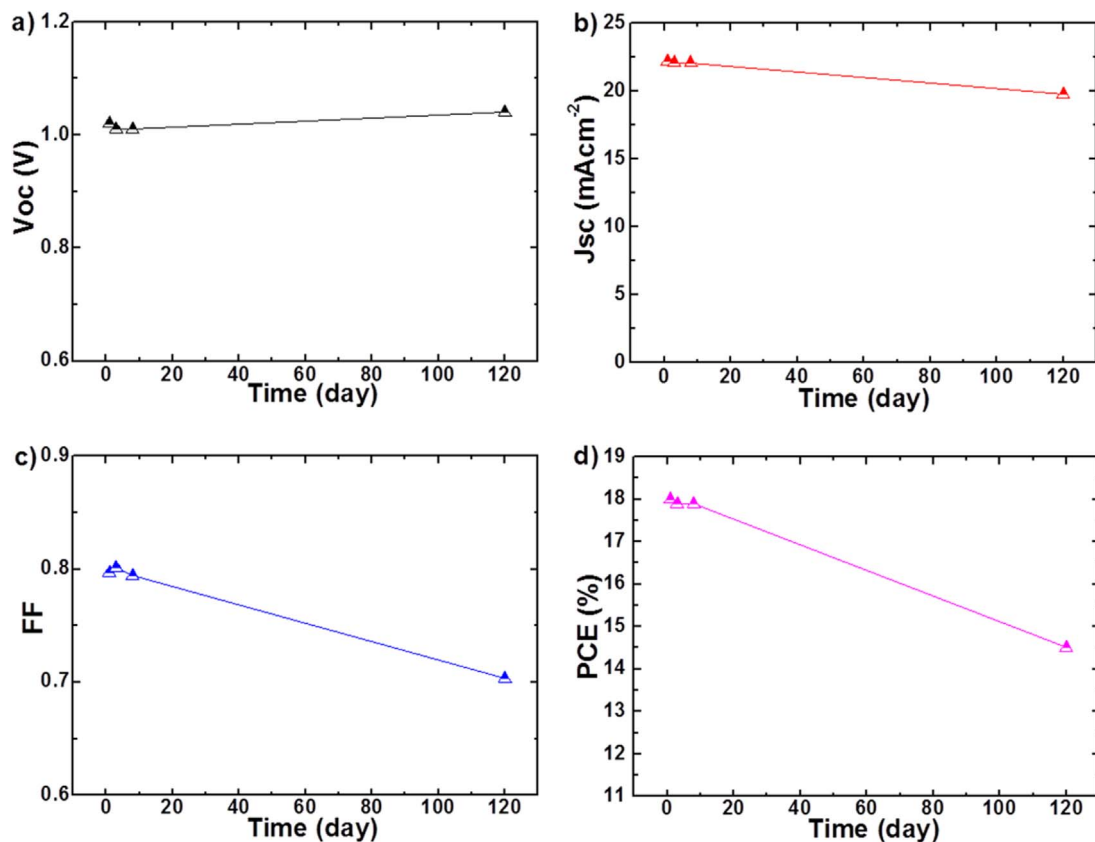


Fig. 7. Device stability of the inverted planar perovskite solar cell of $(\text{FAI})_{0.8}(\text{MABr})_{0.2}\text{PbI}_2$ with a structure of ITO/PBT/ $(\text{FAI})_{0.8}(\text{MABr})_{0.2}\text{PbI}_2/\text{C}_{60}/\text{Ag}$. The test was performed in N_2 -glovebox (O_2 :100 ppm, H_2O : 0.01 ppm, $T=30$ °C) without encapsulation.

4. Conclusion

In conclusion, by using PBT as the interfacial layer, we have fabricated efficient inverted planar perovskites solar cells and systematically studied the effect of Br-doping and FA substitution on the device performance. Higher V_{OC} was realized by Br-doping and an efficiency of 17.3% with a V_{OC} of 1.07 V was obtained from perovskite $\text{MAPbBr}_{0.4}\text{I}_{2.6}$. Further

substitution of “MA” with “FA” lowers the perovskite bandgap which enhances device J_{SC} while maintains higher V_{OC} from Br-doping. A champion efficiency of 18.1% was achieved from $\text{FA}_{0.8}\text{MA}_{0.2}\text{PbBr}_{0.2}\text{I}_{2.8}$ perovskite with stable power output and less hysteresis. This device exhibits long-term stability with only 20% efficiency drop after 4 months in a glovebox without encapsulation. Our results demonstrate highly efficient and stable inverted planar perovskite solar cells can be realized by a

combination of proper interfacial layer and perovskite composition optimization. The high efficiency and long term stability also offer a reference for the applications of the inverted perovskite structure in flexible and tandem solar cells.

Conflict of interest

The authors declare no competing financial interest.

Acknowledgements

The authors gratefully acknowledge the financial support from the National Natural Science Foundation of Jiangsu Province (BK20161514, BK20160887), the National Natural Science Foundation of China (NSFC) (21571106), the National High Technology Research and Development Program ("973" Program) of China (Grant No. 2015CB932200), Synergetic Innovation Center for Organic Electronics and Information Displays.

Appendix A. Supplementary material

Supplementary data associated with this article can be found in the online version at doi:10.1016/j.nanoen.2017.03.001.

References

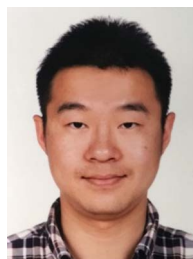
- [1] W. Yin, J. Yang, J. Kang, Y. Yan, S. Wei, *J. Mater. Chem. A* 3 (2015) 8926–8942.
- [2] M. Xiao, F. Huang, W. Huang, Y. Dkhissi, Y. Zhu, J. Etheridge, A. Gray-Weale, U. Bach, Y.B. Cheng, L. Spiccia, *Angew. Chem. Int. Ed. Engl.* 53 (2014) 9898–9903.
- [3] N.J. Jeon, J.H. Noh, Y.C. Kim, W.S. Yang, S. Ryu, S.I. Seok, *Nat. Mater.* 13 (2014) 897–903.
- [4] W.Y. Nie, H.H. Tsai, R. Asadpour, J.C. Blancon, A.J. Neukirch, G. Gupta, J.J. Crochet, M. Chhowalla, S. Tretiak, M.A. Alam, H.L. Wang, A.D. Mohite, *Science* 347 (2015) 522–525.
- [5] Z. Xiao, Q. Dong, C. Bi, Y. Shao, Y. Yuan, J. Huang, *Adv. Mater.* 26 (2014) 6503–6509.
- [6] Z. Xiao, C. Bi, Y. Shao, Q. Dong, Q. Wang, Y. Yuan, C. Wang, Y. Gao, J. Huang, *Energy Environ. Sci.* 7 (2014) 2619–2623.
- [7] Q. Chen, H. Zhou, Z. Hong, S. Luo, H.S. Duan, H.H. Wang, Y. Liu, G. Li, Y. Yang, *J. Am. Chem. Soc.* 136 (2014) 622–625.
- [8] H. Zhou, Q. Chen, G. Li, S. Luo, T. Song, H. Duan, Z. Hong, J. You, Y. Liu, Y. Yang, *Science* 345 (2014) 542–546.
- [9] W. Chen, Y.Z. Wu, Y.F. Yue, J. Liu, W.J. Zhang, X.D. Yang, H. Chen, E.B. Bi, I. Ashrafali, M. Grätzel, L.Y. Han, *Science* 350 (2015) 944–948.
- [10] W. Yan, Y. Li, Y. Li, S. Ye, Z. Liu, S. Wang, Z. Bian, C. Huang, *Nano Energy* 16 (2015) 428–437.
- [11] Z. Zhou, S. Pang, Z. Liu, H. Xu, G. Cui, *J. Mater. Chem. A* 3 (2015) 19205–19217.
- [12] W. Yan, S. Ye, Y. Li, W. Sun, H. Rao, Z. Liu, Z. Bian, C. Huang, *Adv. Energy Mater.* 6 (2016) 1600474.
- [13] P. Docampo, J.M. Ball, M. Darwich, G.E. Eperon, H.J. Snaith, *Nat. Commun.* 4 (2013) 2761.
- [14] N.J. Jeon, J.H. Noh, W.S. Yang, Y.C. Kim, S. Ryu, J. Seo, S.I. Seok, *Nature* 517 (2015) 476–480.
- [15] T.J. Jacobsson, J. Correa-Baena, M. Pazoki, M. Saliba, K. Schenk, M. Grätzel, A. Hagfeldt, *Energy Environ. Sci.* 9 (2016) 1706–1724.
- [16] J.H. Noh, S.H. Im, J.H. Heo, T.N. Mandal, S.I. Seok, *Nano Lett.* 13 (2013) 1764–1769.
- [17] S.D. Stranks, G.E. Eperon, G. Grancini, C. Menelaou, M.J.P. Alcocer, T. Leijtens, L.M. Herz, A. Petrozza, H.J. Snaith, *Science* 342 (2013) 341–344.
- [18] J.H. Heo, S.H. Im, *Nanoscale* 8 (2016) 2554–2560.
- [19] F. Brivio, C. Caetano, A. Walsh, *J. Phys. Chem. Lett.* 7 (2016) 1083–1087.
- [20] N. Pellet, P. Gao, G. Gregori, T. Yang, M.K. Nazeeruddin, J. Maier, M. Grätzel, *Angew. Chem. Int. Ed.* 53 (2014) 3151–3157.
- [21] Y. Li, W. Sun, W. Yan, S. Ye, H. Peng, Z. Liu, Z. Bian, C. Huang, *Adv. Funct. Mater.* 25 (2015) 4867–4873.
- [22] D. Bi, W. Tress, M.I. Dar, P. Gao, J. Luo, C. Renevier, K. Schenk, A. Abate, F. Giordano, J.C. Baena, J. Decoppet, S.M. Zakeeruddin, M.K. Nazeeruddin, M. Grätzel, A. Hagfeldt, *Sci. Adv.* 2 (2016) 1–7.
- [23] L. Gil-Escrig, A. Miquel-Sempere, M. Sessolo, H.J. Bolink, *J. Phys. Chem. Lett.* 6 (2015) 3743–3748.
- [24] W. Yan, Y. Li, Y. Li, S. Ye, Z. Liu, S. Wang, Z. Bian, C. Huang, *Nano Res.* 8 (2015) 2474–2480.
- [25] W. Yan, Y. Li, S. Ye, Y. Li, H. Rao, Z. Liu, S. Wang, Z. Bian, C. Huang, *Nano Res.* 9 (2016) 1600–1608.
- [26] S. Ryu, J.H. Noh, N.J. Jeon, Y.C. Kim, W.S. Yang, J. Seo, S. I. Seok, *Energy Environ. Sci.* 7 (2014) 2614–2618.
- [27] M. Grätzel, *Nat. Mater.* 13 (2014) 838–842.
- [28] J.H. Heo, H.J. Han, D. Kim, T.K. Ahn, S.H. Im, *Energy Environ. Sci.* 8 (2015) 1602–1608.
- [29] T.A. Berhe, W. Su, C. Chen, C. Pan, J. Cheng, H. Chen, M. Tsai, L. Chen, A.A. Dubaleb, B. Hwang, *Energy Environ. Sci.* 9 (2016) 323–356.



Weibo Yan obtained his Ph.D. degree in organic chemistry from Nankai University in 2011. After that, he worked as a postdoctoral fellow in organic nanostructures at Karlsruhe Institute of Technology (KIT) in Germany from 2011 to 2012. From 2013 to 2016, Weibo worked as a postdoctoral fellow in Peking University on the synthesis of solar cell materials and the fabrication of their devices. Since 2016.05, he work as a lecturer in Nanjing University of Posts and Telecommunications, China. His research focuses on photovoltaic devices including perovskite and organic solar cells.



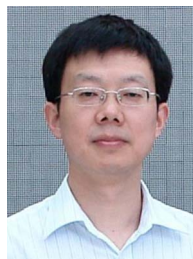
Haixia Rao received her B.S. in Chemistry from Beijing Normal University, China in 2014. She is currently a Ph.D. student in the College of Chemistry and Molecular Engineering, Peking University under the supervision of Assistant Prof. Zuqiang Bian. Her research focuses on photovoltaic devices engineering and physics such as perovskite solar cells.



Chen Wei received his B.S. in Chemistry from Hebei University, China in 2012. He is currently a Ph.D. student in the College of Chemistry and Molecular Engineering, Peking University under the supervision of Assistant Prof. Zuqiang Bian. His research focuses on synthesis of rare earth complexes and application on organic light-emitting diodes (OLEDs).



Zhiwei Liu obtained his Ph.D. degree from Peking University in 2008. After that, he worked as a postdoctoral fellow with Prof. Zhenghong Lu at University of Toronto from 2008 to 2009, and then as a postdoctoral research associate with Prof. Mark E. Thompson at University of Southern California from 2009 to 2011. Now, he is an Associate Professor at College of Chemistry and Molecular Engineering of Peking University, working on organic optoelectronics, including organic light-emitting diodes (OLEDs) and organic photovoltaics (OPVs).



Zuqiang Bian, Ph.D, Associate Professor of College of Chemistry and Molecular Engineering, Peking University, received his Ph.D degree from Beijing Normal University, China in 2002. His research interests focus on rare earth coordination chemistry and the molecular based thin film photo-electronic conversion materials.



Hao Xin is currently a professor of College of Materials Science and Engineering at the Nanjing University of Posts and Telecommunications. She received her Ph.D. from Peking University in 2003. From 2003 to 2006, she worked as a JST CREST researcher at NIMS and a JSPS fellow at JAIST in Japan. Then she moved to USA and worked as an associate researcher and research scientist until 2012 in the Department of Chemical Engineering, University of Washington. Her current research mainly focuses on solution processed thin film photovoltaics including CZTS, CIGS, OPVs, and perovskite solar cells.



Wei Huang obtained his B.S., M.S. and Ph.D. from Peking University, China between 1979 and 1992. After that, he has worked as postdoctor, senior researcher and professor at National University of Singapore from 1993 to 2006. He served as a full professor in Fudan University from 2001 to 2006, and then in Nanjing University of Posts and Telecommunications in China from 2006. He was selected as a member of the Chinese Academy of Sciences in 2011. His present research interests focus on “organic semiconductor materials and optoelectronic devices”, “photoelectric information material and display devices” and “flexible electronics”.